A Saturation Balancing Control Method for Enhancing Dynamic Vehicle Stability

Justin Sill and Beshah Ayalew*
Clemson University-International Center for Automotive Research
Greenville, SC, USA.
Emails: jsill@clemson.edu, beshah@clemson.edu (*corresponding author)

Abstract: This paper proposes a new vehicle stability control method that quantifies and uses the level of lateral force saturation on each axle/wheel of a vehicle. The magnitude of the saturation, which can be interpreted as a slip-angle deficiency, is determined from on-line estimated nonlinear lateral tire forces and their linear projections. Once known, the saturation levels are employed in a saturation balancing control structure that biases the drive torque to either the front or rear axles/wheels with the goal of minimizing excessive under- or over-steer. The control structure avoids the need for an explicit reference model to generate target vehicle responses. The method is particularly suited for a vehicle with a torque-biasing or independent axle or wheel drive system. The benefits of the proposed approach are demonstrated considering a nominally unstable heavy vehicle in an extreme obstacle avoidance type dynamic maneuver.

Keywords: vehicle stability control; saturation balancing; tire force estimation; axle saturation level; independent drive; torque biasing;

1. Introduction

Vehicle stability control (VSC) systems have widely been shown to reduce accidents by minimizing driver's loss of control during aggressive emergency maneuvers. VSC systems manipulate one or more of the front or rear steering inputs, the traction or braking inputs, and/or the tire vertical loads in order to favorably influence the forces and moments generated at the tire-ground interface that affect the lateral and yaw dynamics of the vehicle. The magnitude and direction of control intervention is often determined by calculating deviations from reference/desired vehicle responses such as its yaw rate or lateral acceleration.

The most common VSC (also referred to as vehicle dynamics control (VDC)) systems available on the market today are brake-based systems which extend the functionality of mature hardware technology available for anti-lock braking (ABS) and traction control systems. These systems

1

1. REPORT DATE 01 MAR 2011	2. REPORT TYPE N/A	3. DATES COVERED -

4. TITLE AND SUBTITLE	5a. CONTRACT NUMBER
A Saturation Balancing Control Method for Enhancing Dynamic Vehicle Stability(PREPRINT)	W56HZV-04-2-0001
	5b. GRANT NUMBER
	5c. PROGRAM ELEMENT NUMBER

6. AUTHOR(S)	5d. PROJECT NUMBER
Justin Sill; Beshah Ayalew	5e. TASK NUMBER
	5f. WORK UNIT NUMBER

7. PERFORMING ORGANIZATION NAME(S) AND ADDRESS(ES) Clemson University, Internation Center for Automotive Research, Clemson, SC 29634	8. PERFORMING ORGANIZATION REPORT NUMBER

9. SPONSORING/MONITORING AGENCY NAME(S) AND ADDRESS(ES) US Army RDECOM-TARDEC 6501 E 11 Mile Rd Warren, MI 48397-5000, USA	10. SPONSOR/MONITOR'S ACRONYM(S) TACOM/TARDEC/RDECOM
	11. SPONSOR/MONITOR'S REPORT NUMBER(S) 21548

12. DISTRIBUTION/AVAILABILITY STATEMENT
Approved for public release, distribution unlimited

13. SUPPLEMENTARY NOTES
Submitted for publication in a Special Issue of Int'l Journal of Vehical Design, The original document contains color images.

14. ABSTRACT

15. SUBJECT TERMS

16. SECURITY CLASSIFICATION OF:			17. LIMITATION OF ABSTRACT SAR	18. NUMBER OF PAGES 27	19a. NAME OF RESPONSIBLE PERSON
a. REPORT unclassified	b. ABSTRACT unclassified	c. THIS PAGE unclassified			

facilitate differential (left-to-right) braking on either the front or rear axle to generate a corrective yaw moment on the vehicle for stabilization or for accommodating driver intentions [1-4]. In addition to brake-based systems, VSC can be accomplished by active front/rear steering [5-7]. It can be also achieved by utilizing active suspension components, such as active/semi-active dampers to change tire loads [8]. Finally, VSC can also be achieved using active differentials/transaxle or independent axle/wheel drives to manage or redistribute traction forces for vehicle course corrections [9-15]. The implementation of these alternative, non-brake-based VSC systems is likely to increase in advanced technology vehicles because of certain design benefits. For example, some of these systems help achieve a high degree of maneuverability at low speeds (active steering, active differentials/transaxles, and independent drives), improve handling and ride (active suspensions), and have benefits of packaging convenience (independent drives) for some applications such as wheeled military vehicles.

This paper presents an advanced vehicle stability control (VSC) strategy that is ideally suited for vehicles with torque biasing or independent drive architectures that deliver power individually to each axle or wheel of the vehicle. The core of the proposed VSC strategy is based on identifying the force generation capabilities or saturation levels of the individual axles or wheels on the vehicle and using this information for maintaining the lateral stability of the vehicle. The strategy is motivated by the possibility of applying traction and braking torques (with regenerative braking) at the individual wheels or axles of the vehicle with independent drive or torque-biasing systems. Independent drive systems can be readily configured for emerging power trains in series or parallel electric hybrids, fuel-cell or battery powered electrics or hydraulic-hybrid vehicles. With these systems and the proposed VSC strategy, there is the possibility of enhancing stability and safety while maintaining the efficiency benefits of these systems and preserving driver intentions.

The proposed VSC strategy relies on the estimation of the available lateral and longitudinal force capacity for each axle of the vehicle from available sensors standard on current VSC systems. These sensors include an angular rate sensor for yaw rate, accelerometers for lateral and longitudinal accelerations, and ABS sensors for individual wheel-spins. There are a number of previous research efforts that have addressed the estimation of tire forces and axle slip angles.

2

Perhaps the most common interest has been in the estimation of longitudinal and vertical forces for the purposes of obtaining tire/road friction coefficients. The level of available adhesion is of importance to traction control, ABS, and VSC systems [3, 16-21]. Vertical tire forces (or normal loads) may be estimated by combining static weight distributions and perturbations due to lateral/longitudinal accelerations of the vehicle body and effects of front/rear roll stiffness and damping distributions. Longitudinal tire forces can be estimated using the known applied torque and wheel speed sensor signals of the vehicle, through direct inversion of tire/wheel dynamics [21] or using observer-based methods [20, 22] or extended Kalman filters [16-19].

The estimation of axle lateral forces have been important to recent vehicle dynamics research and are usually coupled with axle slip angle approximations to indirectly characterize the tire behavior that effects the lateral dynamics of the vehicle [16, 18, 19, 21, 23, 24]. The axle lateral forces can be estimated from the lateral acceleration and yaw rate sensors through an inversion of a single-track two degree of freedom handling model [21, 23], an observer [22], or a Kalman filter [16-19, 24]. The axle slip angles may be calculated from an estimate of lateral velocity which is most often achieved by using observers. These estimation efforts have been used in brake-based VSC algorithms [16, 21, 23, 24], but can easily be employed in other VSC schemes like the one proposed in this paper for independent or torque-biasing drives.

This research paper addresses the monitoring and management of axle saturation levels for the purposes of vehicle stability control. Axle saturation will be explicitly estimated and quantified using established tire force estimation schemes. A vehicle stability control structure is then set up to use the identified saturation levels and attempt to rebalance them among the front and rear axles of the vehicle in a manner that corrects understeer and oversteer. Interpretations will be given to the resulting control structure by comparing it against common model-reference VSC systems that use yaw-rate error feedback. While the proposed VSC approach is envisaged to be particularly suited for drive trains featuring independent per-axle and per-wheel drives or torque biasing/biasing systems, the saturation balancing approach could also be adopted for use with brake-based VSC actuation systems. In this paper, we focus primarily on the independent or torque biasing per-axle drive applications and merely highlight the opportunities and challenges for a per-wheel application of the proposed method.

3

The rest of the paper is organized as follows. Section 2 introduced the definition of axle saturation quantities adopted for this work. The details of the 7 DOF vehicle model adopted for the analysis in this paper are postponed to the Appendix. Section 3 details the motivation, interpretation and implementation of the proposed saturation balancing control method. This section also includes a brief discussion on the possible application of the method to a per-wheel saturation balancing control system. Section 4 provides some demonstrative results illustrating the performance of the proposed method. Section 5 summarizes the conclusions of the work and motivates future research.

2. Determination of Axle Saturation

The determination of the saturation levels of the lateral forces at each of the front and rear axles require some way of estimating tire-ground forces. For this purpose, a rigid vehicle handling model, such as the one shown in Figure 1 can be used as a starting point. The definitions of the various force, angle and speed variables shown in Figure 1 are standard and are described in the nomenclature list. The equations of motion derived from this 7 DOF model are also quite standard and are given in summarized form in Appendix A. The model is subsequently reduced to the usual two degree of freedom (bicycle) model consisting of the lateral and yaw equations for the purposes of estimating the lateral tire-ground forces.
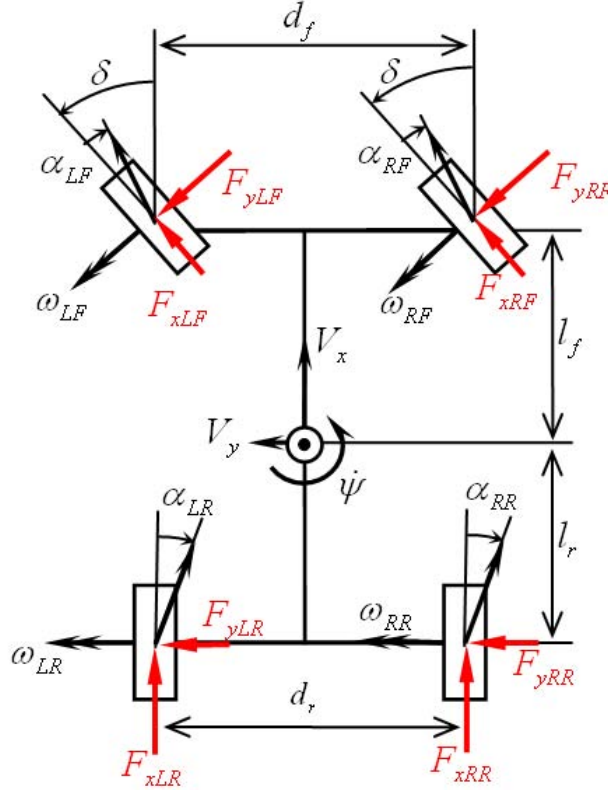
4

Figure 1. Schematic of Vehicle Dynamics Model

The front and rear lateral forces can be determined by inverting the bicycle handling model given measured lateral acceleration, yaw rate and steering angle signals. This approach has been taken in previous works [18, 19, 21-23] where the per-axle lateral forces are estimated from variants of:

$$\begin{Bmatrix} \hat{F}_{yF} \\ \hat{F}_{yR} \end{Bmatrix} = \begin{bmatrix} \cos\delta & 1 \\ l_f\cos\delta & -l_r \end{bmatrix}^{-1} \left\{ \begin{bmatrix} mA_y \\ I_{zz}\dfrac{d\dot\psi}{dt} \end{bmatrix} - \hat{M}_x \right\} \tag{1}$$

where, the hatted variables denote estimates, and:

$$\hat{M}_x = \begin{bmatrix} \sin\delta & \sin\delta & 0 & 0 \\ l_f\sin\delta - \dfrac{d_f}{2}\cos\delta & l_f\sin\delta + \dfrac{d_f}{2}\cos\delta & -\dfrac{d_r}{2} & \dfrac{d_r}{2} \end{bmatrix} \begin{bmatrix} \hat{F}_{xLF} \\ \hat{F}_{xRF} \\ \hat{F}_{xLR} \\ \hat{F}_{xRR} \end{bmatrix}$$

5

In this work, the later term is added to correct for the contribution of the longitudinal forces on the lateral dynamics (from equations (A.2) and (A.3)). This correction uses estimates of these longitudinal forces. There are several approaches for estimating longitudinal tire forces using the controlled torque inputs and the speed sensors for each wheel. These methods range from a simple method that corrects for wheel rotational dynamics through direct differentiation of wheel speed sensor signals, through advanced observer-based methods [20, 22]. Here, for our purposes, we use the simple method for longitudinal force estimation:

$$\hat{F}_{xi} = \left(T_i - I_w \frac{d\omega_i}{dt} \right) \Big/ R_w \tag{2}$$

where, ω_i is the measured wheel speed, T_i is the applied torque, and I_w & R_w are the tire/wheel inertia and effective tire radius.

Axle slip angles can be determined through an observer (or Kalman filter) by estimating lateral velocity from the lateral acceleration, longitudinal velocity, and yaw rate sensors. For example, lateral velocity estimation can be setup as [3, 21]:

$$\frac{d}{dt}\hat{V}_y = \hat{A}_y - \dot{\psi}V_x + K_y\left(A_y - \hat{A}_y\right) \tag{3}$$

where, $\hat{A}_y = \dfrac{\hat{F}_{yF} + \hat{F}_{yR}}{M}$ and $\dot{\psi}, V_x,$ & A_y are the measured yaw rate, speed, and lateral acceleration of the vehicle, while K_y is an observer gain. The estimated axle slip angles can then be obtained from the kinematic relations:

$$\hat{\alpha}_F = \tan^{-1}\left(\frac{\hat{V}_y + l_f\dot{\psi}}{V_x} \right) - \delta \tag{4}$$

$$\hat{\alpha}_R = \tan^{-1}\left(\frac{\hat{V}_y - l_r\dot{\psi}}{V_x} \right) \tag{5}$$

Knowing estimates of the axle lateral forces and slip angles at each instant, a definition of the saturation level of the axle, α_{sat}, can be given using the illustration in Figure 2.
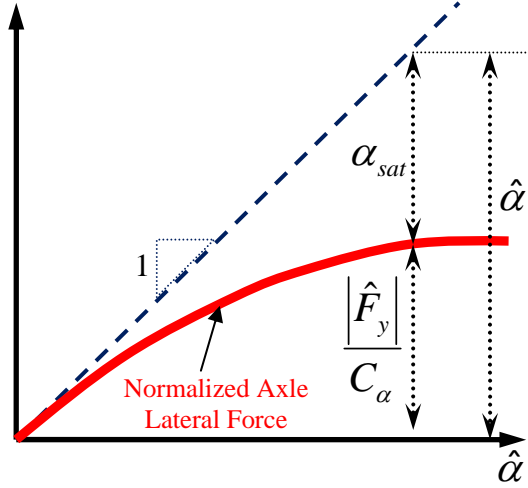
6

Figure 2. Definition of Axle Saturation

Assuming that the axle cornering stiffness is a known constant, the axle saturation can be defined as the difference between the normalized estimate of the nonlinear axle lateral force (which has the dimensions of slip angle) and the prevailing estimated slip angle:

$$\alpha_{sat} = \hat{\alpha} - \frac{\hat{F}_y}{C_\alpha} \tag{6}$$

The axle saturation defined by equation (6) can be interpreted as a slip angle deficiency of the nonlinear lateral force $\hat{F}_y$ from that of the linear force F'_y expected from cornering stiffness considerations, i. e., $F'_y = C_\alpha \hat{\alpha}$.

It should be mentioned that, while we consider the cornering stiffness to be constant for the purpose of discussing the axle saturation approach in this paper, this may not be fully adequate for all situations. For example, as lateral acceleration levels change on different road surfaces the amount of lateral load transfer also changes. It is well known that depending on the selected tire, lateral load transfers could reduce the effective cornering stiffness of the axle. Therefore, an axle cornering stiffness estimation scheme would be required for real-world implementation of the strategy we propose here. These aspects are neglected for now for simplicity of exposition of the saturation balancing schemes for stability control.

7

3. Axle Saturation balancing Control

3.1 Motivation and Interpretation

It is important to note that the saturation of the front and rear axles may occur at different rates and magnitudes. This difference in the saturation levels provides a direct indication of the occurrence of understeer and oversteer behavior for the vehicle. For example, when the front axle saturation is larger than the rear axle saturation ($\alpha_{satF} > \alpha_{satR}$) the vehicle is experiencing more understeer as shown in Figure 3. Conversely, a more oversteering vehicle can be observed as the rear axle saturates more than the front ($\alpha_{satF} < \alpha_{satR}$). Ideally, equal saturation of the front and rear axles avoids excessive under or oversteer for the vehicle. To demonstrate this, the geometric equation representing the cornering of a single track vehicle can be used [25-28].

$$\delta = \frac{L}{R} + \left(\alpha_F - \alpha_R\right) \tag{7}$$

Substituting (6) into (7):

$$\left(\alpha_F - \alpha_R\right) \cong \left(\alpha_{sat,F} + \frac{\hat{F}_{y,F}}{C_{\alpha,F}}\right) - \left(\alpha_{sat,R} + \frac{\hat{F}_{y,R}}{C_{\alpha,R}}\right) = \left(\alpha_{sat,F} - \alpha_{sat,R}\right) + \left(\frac{\hat{F}_{y,F}}{C_{\alpha,F}} - \frac{\hat{F}_{y,R}}{C_{\alpha,R}}\right) \tag{8}$$
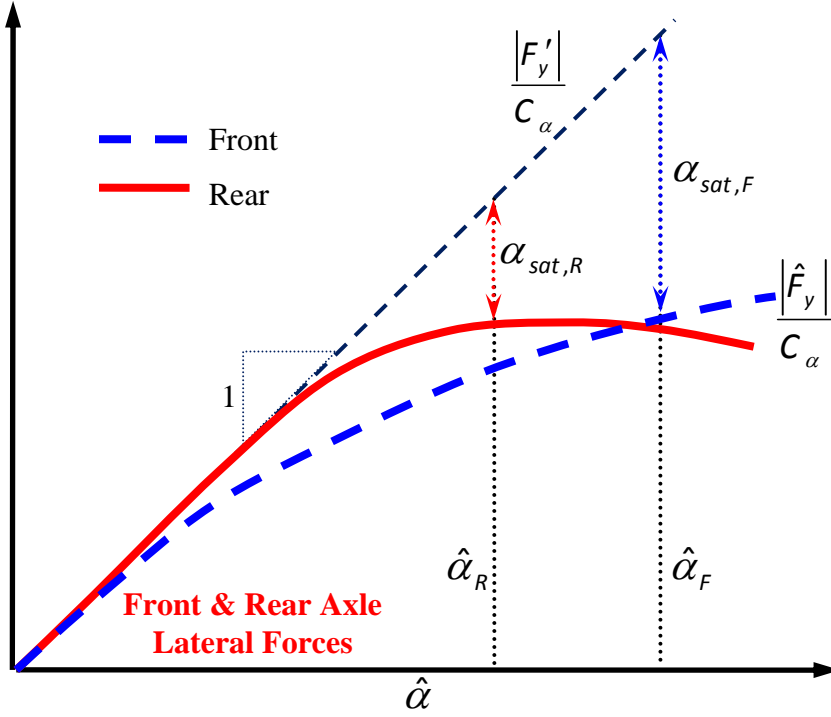
8

Figure 3. Under Steering Vehicle Axle Force Saturation

From the illustration in Figure 3, the assumption of a linear tire for α_F and α_R would have resulted in:

$$\underbrace{\left(\alpha_F - \alpha_R\right)}_{\text{Linear tire}} = \underbrace{\frac{F'_{y,F}}{C_{\alpha,F}} - \frac{F'_{y,R}}{C_{\alpha,R}}}_{\text{Linear tire}} \tag{9}$$

Comparing equations (8) and (9), it can be seen that minimizing the differences in the saturation levels would leave a more linear behavior for the differences in axle slip angles. This suggests the possibility of using the differences in axle saturation levels (axle saturation differential) for feedback control with the goal of reducing slip angle differentials between the axles. If the front/rear axle saturation level differential is kept near zero, then it may be expected that a vehicle with nonlinear tires can be made to behave like one with linear tires. The extent of the saturation level differential may be used by a saturation balancing controller to identify occurrences of nonlinearity and take appropriate actions to approximate the desirable

9

predictability of a linear response as best as possible. Linear response is expected and easily perceived by most drivers.

Unlike in previous research, where axle saturation was largely considered an undesirable behavior to be avoided through controller intervention [21], the above derivation suggests that per axle saturation can be managed through a rebalancing of saturation levels in order to facilitate predictability of the response and in so doing achieve stability and safety without degrading driver intentions. It is also possible that this saturation balancing approach leads to more efficient use of the tires (and possibly the drive/actuation system) by redirecting actuation efforts to the responsive axles/tires. In other words, it attempts to use each axle to its capacity.

3.2 Implementation of Saturation balancing Control

In this section, a vehicle stability control strategy employing axle saturation information is outlined. The proposed process is summarized in Figure 4. First, the axle lateral force capacity, axle slip angles and the axle saturation levels are estimated online as described in Section 2 from available vehicle dynamics sensors. This saturation levels can then be used to determine the required corrective yaw moment to minimize the saturation differentials. As discussed earlier, there exist many activation systems including brake-based, torque vectoring, independent drive, or active steer systems that may be used to generate the corrective yaw moment on the vehicle. In the present work, the required yaw moment will be achieved by biasing the drive torque distribution between the front and rear axles in such a way as to re-balance the axle saturation levels.
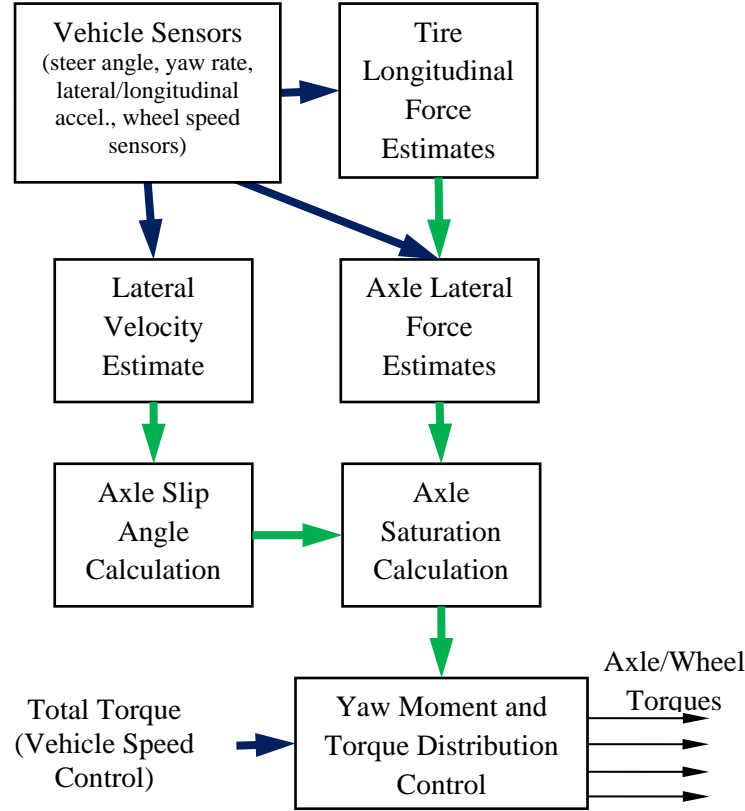
Figure 4. Implementation of the Saturation balancing Control Scheme

There are many possible feedback control structures that may use the axle saturation differential for vehicle stability control including PID forms, sliding mode, fuzzy-logic, or optimal controllers. Here, as an example, the corrective yaw moment maybe defined by a PID form using the difference between the front/rear axle saturation levels:

$$M_\psi = \left(K_P + \frac{K_I}{s} + K_D s \right) \left(\alpha_{satF} - \alpha_{satR} \right) \tag{10}$$

It should be noted that this saturation balancing controller does not need an explicit reference model to generate a desired/target response. It turns out that this control law may be given interpretations by comparing it to the common yaw rate error -based vehicle stability control systems that generate the corrective yaw moment as [3, 4]:

11

$$M'_{\psi} = \left(K'_P + \frac{K'_I}{s} + K'_D s \right) \left(\dot{\psi} - \dot{\psi}_{desired} \right)$$ (11)

where, $\dot{\psi}_{desired}$ is a desired yaw rate generated from a reference model. It is often taken to be the steady state yaw rate from a linear bicycle model at speed V_x and steering input δ. It is given by:

$$\dot{\psi}_{desired} = \frac{V_x \delta}{L + (K_{us}V_x{}^2)/g}$$ (12)

K_{us} is the understeer gradient computed from the axle cornering stiffness's and vehicle c.g locations [26].

There is a key difference between the two vehicle stability control forms (10) and (11) when it comes to practical implementation. The implementation of the yaw rate error control (11) often requires enforcing limitations for the maximum allowable (desired) yaw rate that bounds the otherwise unbounded desired yaw rate obtained from the linear steady state model ($\dot{\psi}_{desired}$). We now show that the axle saturation balancing approach enforces an internal limit that is based on the online estimated capability of the nonlinear tires. Substituting equations (4-5) into (6), the front/rear axle saturation differential is given by:

$$\begin{aligned}
\left(\alpha_{satF} - \alpha_{satR} \right) &= \left(\hat{\alpha}_F - \frac{\hat{F}_{y,F}}{C_{\alpha,F}} \right) - \left(\hat{\alpha}_R - \frac{\hat{F}_{y,R}}{C_{\alpha,R}} \right) \\
&= \tan^{-1}\left(\frac{\hat{V}_y + l_f \dot{\psi}}{V_x} \right) - \delta - \frac{\hat{F}_{y,F}}{C_{\alpha,F}} - \tan^{-1}\left(\frac{\hat{V}_y - l_r \dot{\psi}}{V_x} \right) + \frac{\hat{F}_{y,R}}{C_{\alpha,R}}
\end{aligned}$$ (13)

Considering small angles (order of 10 degrees), this reduces to:

$$\left(\alpha_{satF} - \alpha_{satR} \right) \approx \frac{L\dot{\psi}}{V_x} - \left(\delta + \frac{\hat{F}_{y,F}}{C_{\alpha,F}} - \frac{\hat{F}_{y,R}}{C_{\alpha,R}} \right)$$ (14)

By analogy with the yaw rate error used in equation (11), we can define an "equivalent" desired yaw rate that is implicit in the saturation balancing controller in equation (10) as:

12

$$\dot{\psi}'_{desired} = \left(\delta + \frac{\hat{F}_{y,F}}{C_{\alpha,F}} - \frac{\hat{F}_{y,R}}{C_{\alpha,R}} \right) \frac{V_x}{L} \qquad (15)$$

This shows that the saturation balancing approach internalizes the computation of a desired yaw rate which is inherently related to the prevailing nonlinear force estimates. No explicit limitation of the desired yaw rate would be required in this case.

The "equivalent" desired yaw rate can also be given a value associated with the lateral force coefficient. Substituting $\hat{F}_y = \mu_y F_z$ in (14), where F_z is the axle normal load:

$$\dot{\psi}'_{desired} = \left(\delta + \frac{\mu_{y,F} F_{z,F}}{C_{\alpha,F}} - \frac{\mu_{y,R} F_{z,R}}{C_{\alpha,R}} \right) \frac{V_x}{L} \qquad (16)$$

For the case with $\mu_{y,F} = \mu_{y,R} = \mu_y$, the "equivalent" desired yaw can be written in-terms of the understeer gradient and the force coefficient:

$$\dot{\psi}'_{desired} = \left(\delta + \mu_y K_{us} \right) \frac{V_x}{L} \qquad (17)$$

The peak lateral friction coefficient is often assumed constant in controlled studies; however variations do occur on different road surfaces and in changing weather conditions. The corrective yaw moment derived from axle saturation error (equation (10)) internally accounts for these variations by linking the equivalent desired yaw rate to the saturating behavior of the tires/axles. As a consequence of saturation balancing control, as the driver steer angle input increases, the 'equivalent' desired yaw rate is altered based on the available lateral friction, vehicle velocity, wheelbase, and understeer gradient as given by equation (17) and illustrated in Figure 5. This is an added benefit of the axle saturation balancing control strategy, since it does not require explicit estimation of the tire-road friction coefficient to take into account limitations from the saturating behavior of the tires.
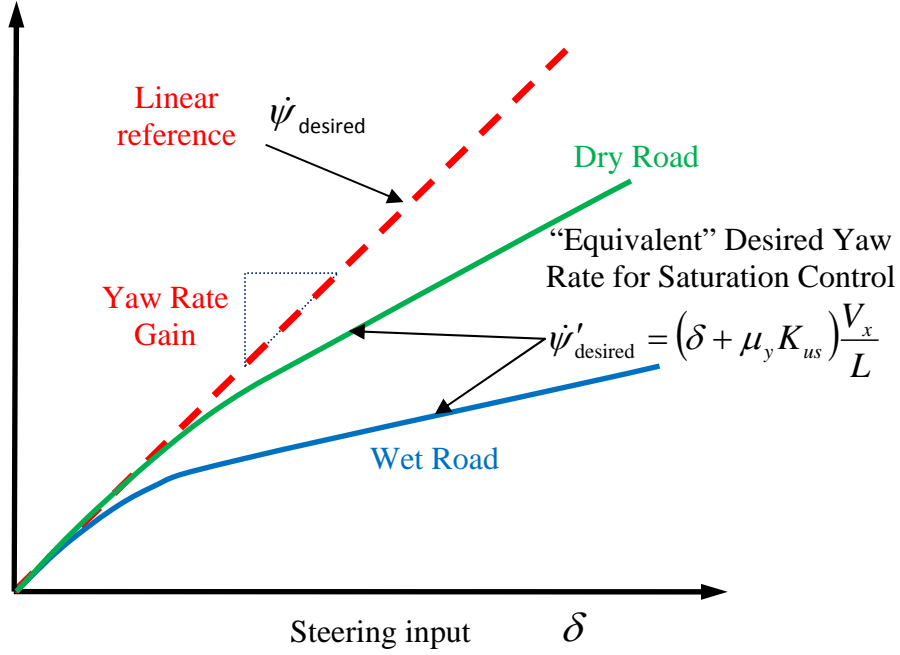
Figure 5. 'Equivalent' Desired Yaw Rate Used Internally by the Saturation balancing Control

The inclusion of the nonlinear tire properties in the saturation balancing controller allows easy adaptation of the vehicle to sudden decreases in tire-road friction coefficients or to sudden decreases in speed by internally reducing the "equivalent" desired yaw rate.

3.3 Torque Biasing Control

The corrective yaw moment generated via equation (10) is re-interpreted for an independent axle drive or torque-vectoring application. A torque biasing PI control can be defined from the balance of the front/rear axle saturation levels as follows:

$$\lambda = \left(K_P + \frac{K_I}{s} \right)\left(\alpha_{satF} - \alpha_{satR} \right) + \lambda_0 \qquad (18)$$

And this can be compared with a torque biasing PI control that uses yaw rate error feedback:

14

$$\lambda = \left(K_P' + \frac{K_I'}{s} \right) \left(\dot{\psi} - \dot{\psi}_{desired} \right) + \lambda_0 \qquad (19)$$

In both cases, λ is the percent of net torque to the rear axle (limited within the range of 0 and 100%), and λ_0 is the initial torque bias for which no stability control action is applied. The total torque T_{total} is computed and tuned separately so as to maintain the desired forward speed. The front and rear axle torques are given by:

$$T_F = T_{total} \times (1 - \lambda) \quad \text{and} \quad T_R = T_{total} \times \lambda \qquad (20)$$

With this torque distribution, excessive vehicle understeer, defined by more saturation on the front than rear axle, may be corrected by this controller through increased rear torque bias. Conversely, excessive oversteer is corrected through front torque bias as shown for a left turn in Figure 6 (red indicates saturating axle/tires).
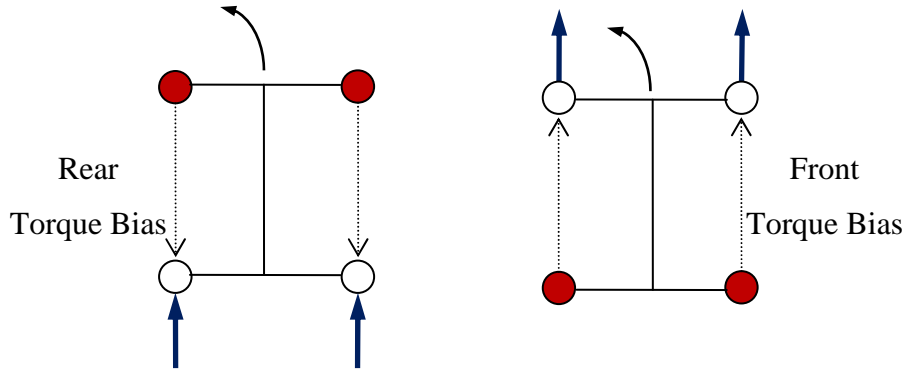
Rear
Torque Bias

Front
Torque Bias

Figure 6. Control Activation for a Left Turn (Red indicates saturating tires)

3.4 Extension to Per-Wheel Application

It has been discussed so far that a per-axle saturation balancing VSC strategy may successfully stabilize and correct the course of a vehicle in destabilizing situations. However, this method does not consider the capacity of individual tires to make such corrections. The corrective wheel torques (in braking or traction) might be inadequate in conditions where the individual tires (not axles) saturate. Therefore, it is natural to consider extending the concept of saturation balancing to a per-wheel strategy where the saturation levels will be quantified for each individual tire.

15

Such a per-wheel strategy would have potential benefits of reducing uneven tire wear, through an equal usage of tire capacity, and lowering the magnitudes of the stabilizing braking/traction torques. The later aspect may also reduce the need for activation of lower level controllers for avoiding wheel lockup or spin.

Despite the above attractive benefits, estimation and definition of individual tire saturation levels is not quite trivial. To define and determine individual tire saturation levels, more detail is required in the estimations as compared to what has been discussed for estimation of the axle saturation levels. While the required estimations for most of the forces and slip angles follows along the lines described above for the per-axle strategy, the slip angle estimation and lateral force estimation must be modified to separate action on the left and right tires. The separation of lateral force axle estimation into individual left and right tire contribution is a significant challenge that has been recognized (but not adequately solved) in previous research by [18, 19]. It is envisioned that an appropriate tire model may be used to separate the lumped axle lateral force estimates above into contributions from the left and right side tires. In addition, new definitions of tire saturation levels that consider the combined longitudinal and lateral slip at each tire are expected to enhance the possible benefit of this per-wheel saturation balancing approach. The authors expect to present results from this approach in a future publication.

4. Results and Discussions

The per-axle saturation balancing method and the common yaw rate error-based stability control method were applied to a medium duty truck with a GVW of 8000 lbs and with an upgraded power train featuring independent wheel drives. The vehicle considered is a nominally over steering vehicle (considered a worst-case scenario) with font-rear distributions of 55%-45% in weight, 35%-65% in initial drive and 40%-60% in roll stiffness, and on dry (μ_{peak}=1.0) and wet (μ_{peak}=0.6) asphalt road. The mathematical vehicle model exercised in these analyses is the one summarized in the Appendix.

To evaluate the handling performance in aggressive maneuvers, a "sine with dwell" steering angle input was considered. This open-loop maneuver has been defined by NHTSA in the US to emulate a severe obstacle avoidance type maneuver for evaluating VSC systems [29]. This input

induces a dynamic nonlinear vehicle response, which causes high vehicle sideslip for an uncontrolled vehicle as seen by the baseline simulations in Figure 7 for a speed of 100 kph.

The saturation balancing and yaw rate error control strategies described in Section 3.3 are evaluated and compared with control gains selected to utilize the range of available torque-biasing within the limits of 0% and 100% (normalized values between 0 and 1) on the front and rear axles while minimizing the occurrence of torque-biasing limits (minimal actuator saturation for each strategy). The uncontrolled and controlled responses of the vehicle on dry asphalt can be seen in Figure 7. It should be noted that the desired yaw rate is used only with the yaw rate error-based strategy, and is given by equation (12).
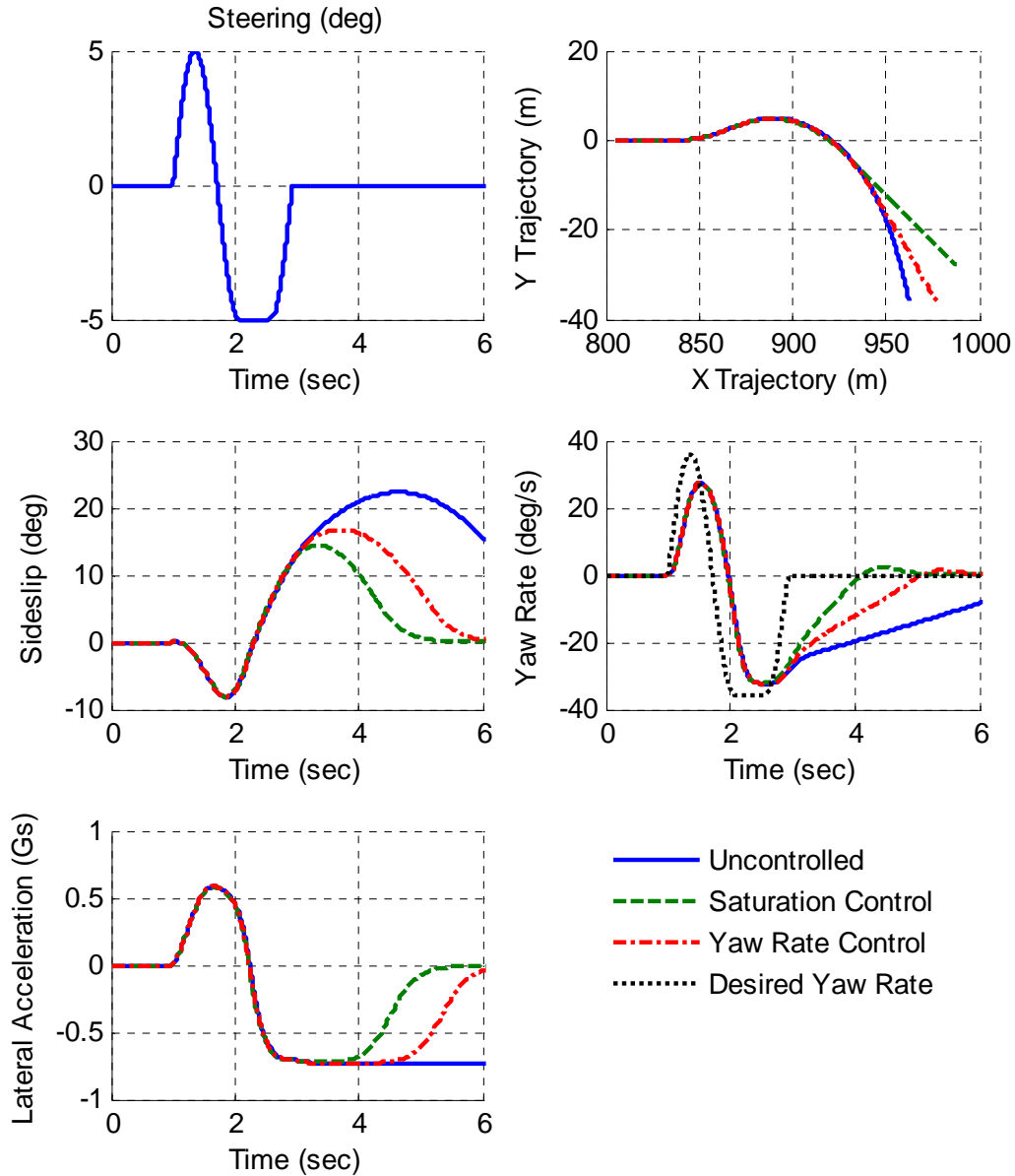
17

Figure 7. Response for Uncontrolled and Controlled Vehicle on Dry Asphalt ($\mu_{peak}=1.0$)

It can be seen in Figure 7 that both the saturation balancing and yaw rate error controllers reduce the sideslip of the vehicle as it concludes the maneuver. This can also be seen by the return of the yaw rate, side-slip angle and lateral acceleration responses to zero. The saturation balancing controller does perform better than the yaw rate error controller as exhibited by the quicker return of the sliding vehicle to on-center. The corresponding controller activity (rear torque bias) for each strategy is shown in Figure 8.
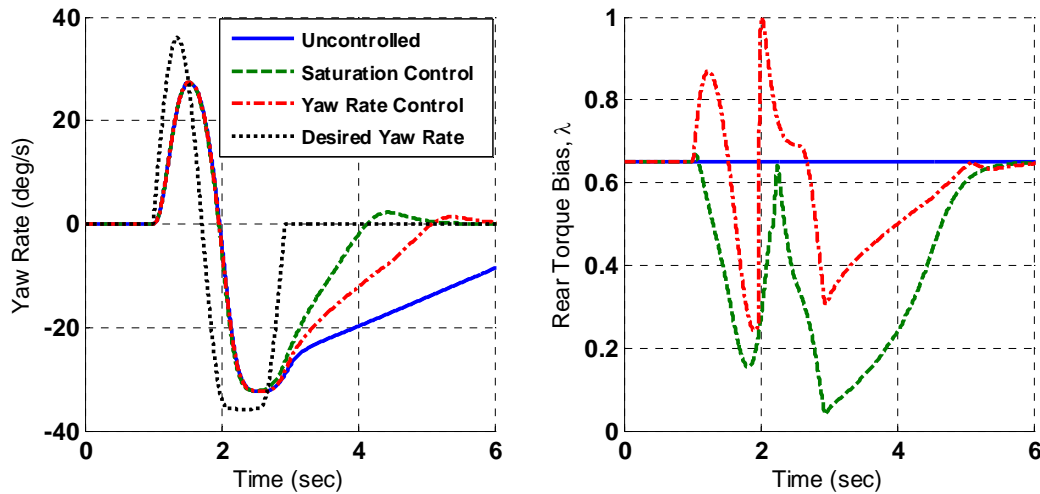
18

Figure 8. Yaw Rate and Torque Bias for Uncontrolled and Controlled Vehicle on Dry Asphalt (μ_{peak}=1.0)

At the start of the maneuver, the saturation rebalancing control transfers torque-bias briefly to the rear axle but it quickly reverses the bias to the front axle (reduce rear bias), while the yaw rate control acts contrary by requesting more rear torque-bias. Since this vehicle is (nominally) slightly oversteer, the saturation rebalancing controller seeks to balance the usage of the tires on the front and rear axles by quickly generating a yaw moment that will induce understeer (front bias). However, the yaw rate control sees a deficiency of yaw rate from the desired (merely pre-determined from equation 12) and acts to produce a yaw moment to increase the vehicle's yaw. These differences in activations have only small differences in their effects concerning the achievable yaw rate or trajectory of the vehicle early in the maneuver, but do show an impact on the different vehicle responses observed in later more severe part of the maneuver involving high vehicle and tire side slip angles.

It is known that the performance of VSC systems can be negatively affected as a vehicle transverses road surfaces of lower friction coefficients, such as wet asphalt. To evaluate the performance and effectiveness of the two vehicle stability controllers on such a surface, the above maneuver is repeated using tire data with a peak friction coefficient of μ_{peak}=0.6. As the maneuver above on dry asphalt was selected to be extreme, it is expected that the vehicle should exhibit responses with lower magnitudes on wet asphalt because of the physical tire adhesion

19

limits. The responses of the uncontrolled and controlled vehicle under the two controllers on wet asphalt are shown in Figure 9.
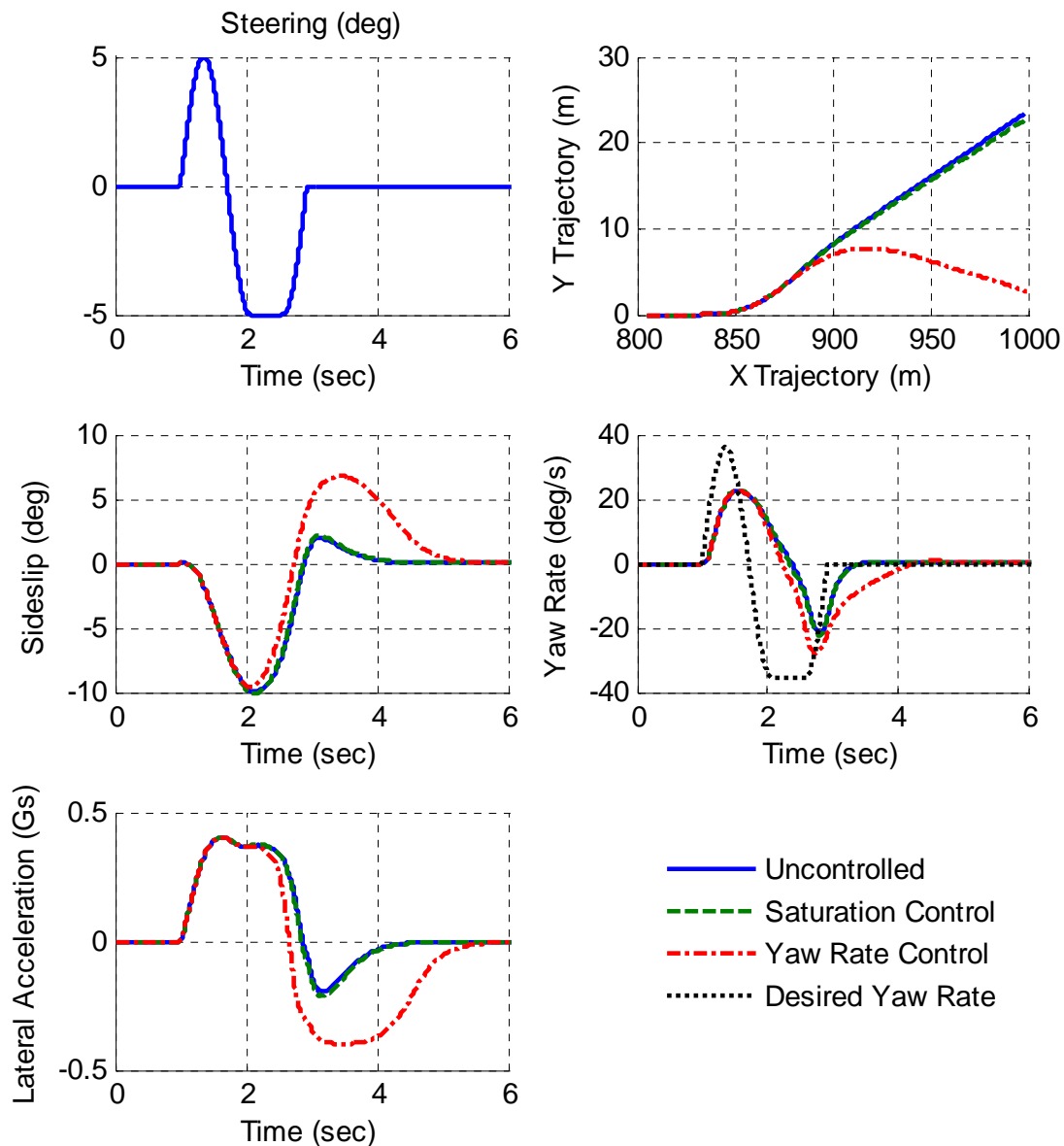

Figure 9. Response for Uncontrolled and Controlled Vehicle on Wet Asphalt ($\mu_{peak}=0.6$).

The yaw rate error control does not adapt to the lower friction coefficient but strives to track predetermined desired yaw rate which is not limited by the severely saturating tires on this surface. This leads to large sideslip of the vehicle for a prolonged period after the conclusion of the maneuver. The saturation balancing control, on the other hand, considers the reduction in

20

lateral force capacity and limits the vehicle sideslip angle. This behavior achieved with the saturation balancing controller allows the vehicle to quickly recover to straight ahead at the end of the maneuver. The quick return of the saturation balancing controller is very desirable from a driver's perspective and from traffic safety point of view. It means lane changes and obstacle avoidance could be executed smoothly and swiftly without alarming the driver by taking too much time in responding to his/her steering commands.

The torque-bias activations of the two stability controllers for the maneuver on wet asphalt are shown in Figure 10. The saturation balancing controller achieves the observed response with lower overall swings in the torque bias except at the initial turn in. This desirable aspect can be attributed to the fact that, with the saturation balancing controller, controller interventions are needed mainly to alleviate differences in axle saturation levels which do not necessarily command as much torque bias as trying to track some reference/desired yaw rate projected from a reference steady state handling model. The actual yaw rate response tracks the reference very poorly as shown in the Figure 10.
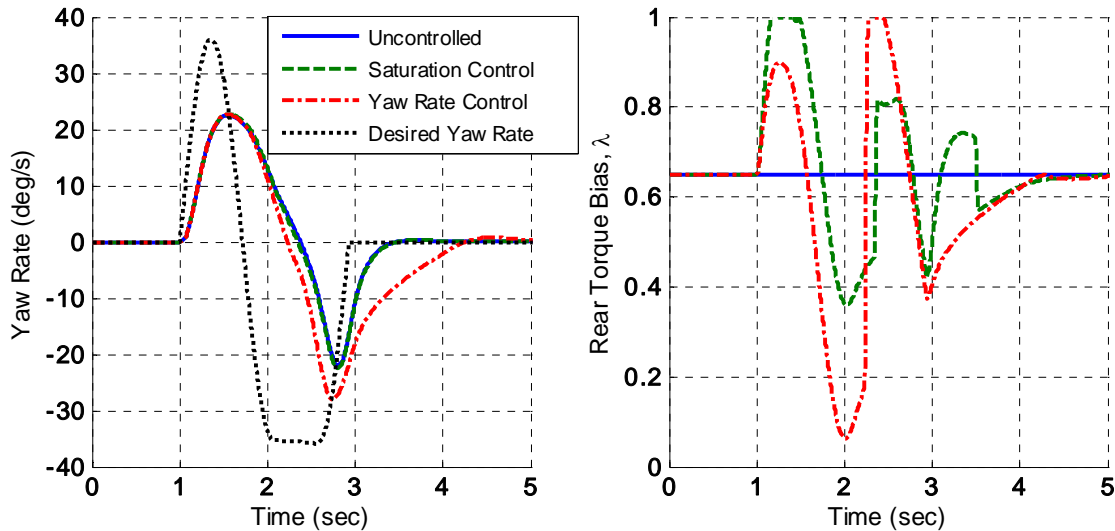

Figure 10. Yaw Rate and Torque Bias for Uncontrolled and Controlled Vehicle on Wet Asphalt (μ_{peak}=0.6)

Finally, one can also look at the individual axle saturation levels during the manoeuvre to get a sense of the operating points of the two control strategies. These are shown in Figure 11 for the case of wet asphalt for the same manoeuvre considered above. It can be seen that in the later

parts of the manoeuvre the yaw rate based controller causes large axle saturation levels while the saturation balancing controller manages these to low levels. Despite this, it should be emphasized that the control strategy acts on the axle saturation differential between the front and rear axles and not on the individual axle saturation levels.
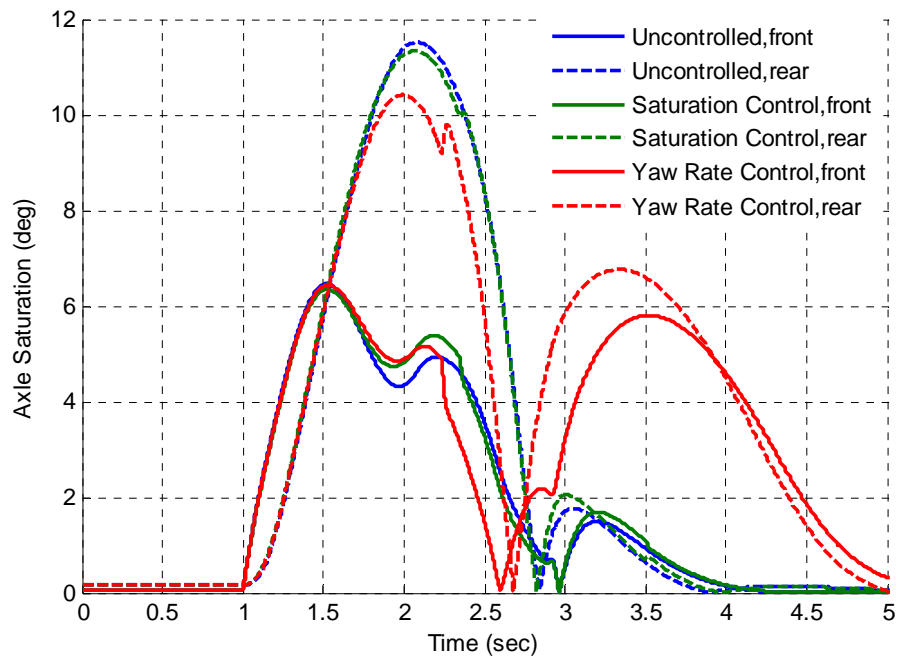

Figure 11. Front and Rear Axle Saturations for Uncontrolled and Controlled Vehicle on Wet Asphalt (μ_{peak}=0.6)

5. Conclusions

In this paper, a vehicle stability control strategy that quantifies and uses axle saturation levels is presented and compared to an established yaw rate error-based approach. The computation of the saturation levels is based on commonly available vehicle dynamics sensors and established force and slip angle estimation methods. The following observations are made regarding the axle saturation balancing control strategy proposed and analyzed in this paper.

- The saturation balancing control method attempts to mimic desirable linear response by minimizing nonlinear contributions from the saturating behavior of the tires on a two-axle vehicle.

22

- Unlike the established yaw rate error-based approaches, the saturation balancing controller does not use an explicit reference model to generate a desired/target response. However, it is shown that the saturation balancing control method internally uses an 'equivalent' desired or target yaw rate that takes into account the nonlinear tire force estimates. In so doing, the method also accounts for and accommodates variations in tire-road friction without explicitly computing a friction coefficient.

- Computed axle saturation levels in an aggressive maneuver negotiated with the axle saturation balancing controller and the baseline yaw rate error-based controller indicate that the former is better at managing the axle saturation levels.

This work indicated that the utilization of axle saturation differentials in vehicle stability control systems has merit. It has also been highlighted that extending this to the case of a per-wheel saturation balancing strategy may provide added benefits in more efficient tire use, more even tire wear and reduced energy (torque) need for the purpose of stabilizing the vehicle. The authors seek to address this strategy in a future work.

Appendix: System Modeling

Detailed derivations and discussions of the 7 DOF vehicle model used in this paper are given in [11, 12, 25]. The notations used below are defined in the nomenclature below and in Figure 1.

The longitudinal, lateral, and yaw equations of motion are, respectively:

$$m(\dot{V}_x - V_y\dot{\psi}) = \sum F_x = (F_{xLF} + F_{xRF})\cos(\delta) - (F_{yLF} + F_{yRF})\sin(\delta)$$
$$+ F_{xLR} + F_{xRR} - \frac{1}{2}\rho C_D A V_x^2 - mgC_{rr}$$

(A.1)

$$m(\dot{V}_y + V_x\dot{\psi}) = \sum F_y = (F_{yLF} + F_{yRF})\cos(\delta) + (F_{xLF} + F_{xRF})\sin(\delta)$$
$$+ F_{yLR} + F_{yRR}$$

(A.2)

$$I_{zz}\ddot{\psi} = \sum M_z = l_f[(F_{yLF} + F_{yRF})\cos(\delta) + (F_{xLF} + F_{xRF})\sin(\delta)] + l_r(F_{yLR} + F_{yRR})$$
$$+ \frac{d_f}{2}[(F_{xRF} + F_{xLF})\cos(\delta) + (F_{yLF} - F_{yRF})\sin(\delta)] + \frac{d_r}{2}(F_{xRR} - F_{xLR})$$

(A.3)

23

The tire/wheel dynamics are given by:

$$I_w \dot{\omega}_i = T_{w,i} - F_{x,i} R_w \qquad (A.4)$$

where i represents LF, RF, LR, and RR tires.

The vertical loads for the left front and left rear tires, that are required for the tire model, are given by (others follow similarly):

$$F_{zLF} = \frac{mgl_r}{2L} - A_x\left(\frac{mh_{cg}}{2L}\right) - A_y\left(\frac{ml_r h_{rcF}}{Ld_f} + \frac{m(h_{cg} - h_{rcF})K_{\phi F}}{d_f(K_{\phi F} + K_{\phi R} - mg(h_{cg} - h_{rcF}))}\right) \qquad (A.5)$$

$$F_{zLR} = \frac{mgl_f}{2L} + A_x\left(\frac{mh_{cg}}{2L}\right) - A_y\left(\frac{ml_f h_{rcR}}{Ld_r} + \frac{m(h_{cg} - h_{rcR})K_{\phi R}}{d_r(K_{\phi F} + K_{\phi R} - mg(h_{cg} - h_{rcR}))}\right) \qquad (A.6)$$

The tire slip ratios and slip angles are computed as:

$$\kappa_i = \frac{\omega_i R_w}{V_{xi}} - 1 \qquad (A.7)$$

$$\alpha_{LF} = \tan^{-1}\left(\frac{V_y + l_f \dot{\psi}}{V_x + \frac{d_f}{2}\dot{\psi}}\right) - \delta \text{ and } \alpha_{LR} = \tan^{-1}\left(\frac{V_y - l_f \dot{\psi}}{V_x + \frac{d_f}{2}\dot{\psi}}\right) \qquad (A.8)$$

Since longitudinal tractive forces of each wheel are to be exploited to influence the lateral handling dynamics, a proper tire model that considers combined slip conditions (longitudinal and lateral) must be used, i.e. models that give $F_x = F_x(\kappa, \alpha, F_z)$ and $F_y = F_y(\kappa, \alpha, F_z)$ are needed. For this purpose, combined-slip tire data provided in [30] was suitably scaled by tire size/load and implemented as a multi-dimensional lookup table.

Nomenclature

α_i = lateral slip angle of tire *i*
$\alpha_{sat,i}$ = saturation of tire *i*
δ = road wheel steering angle
κ_i = longitudinal slip of tire *i*
ρ = density of air

24

$\dot{\psi}$ = vehicle yaw rate

λ = rear torque bias

λ_0 = initial rear torque bias

ω_i, = rotational speed of wheel i

μ = friction coefficient

A = vehicle frontal area

A_x, A_y = longitudinal and lateral acceleration

$C_{\alpha,F}$, $C_{\alpha,R}$ = front/rear axle cornering stiffnesses

C_D= drag coefficient

C_{rr}= rolling resistance coefficient

F_x = longitudinal tire force

F_y = lateral tire force

F_z = normal tire load

g= gravitational constant

h_{cg} = vehicle C.G. height

h_{rcF}, h_{rcR} = front/rear roll center height

I_{zz} = yaw inertia

I_w = inertia of motor/wheel referred to wheel

$K_{\phi R}$, $K_{\phi L}$ = rear/front roll stiffness

K_P, K_I, K_D = controller gains

L= wheel base

l_f, l_r =distance of front/rear axle from vehicle C.G.

m = total vehicle mass

R_w = effective wheel radius

d_f,d_r = front/rear wheel track width

T_f, T_r = front/rear axle torques

T_{total} = total wheel torque

$T_{w,i}$ = individual wheel torque

V_x = longitudinal velocity in vehicle x-axis

V_y = lateral velocity in vehicle y-axis

References

1.   Ghoneim, Y., W. Lin, D. Sidlosky, H. Chen, Y.-K. Chin, and M. Tedrake, "Integrated Chassis Control System to Enhance Vehicle Stability". International Journal of Vehicle Design, 2000. **23**: p. 124-144.

2.   Rajamani, R., Vehicle Dynamics and Control. Springer, 2006.

3. Tseng, H.E., B. Ashrafi, D. Madau, T. Allen Brown, and D. Recker, "The development of vehicle stability control at Ford". IEEE/ASME Transactions on Mechatronics, 1999, **4**(3): p. 223-234.

4. Van Zanten, T., "Bosch ESP Systems: 5 Years of Experience", in SAE Automotive Dynamics & Stability Conference, Troy, MI , SAE paper number 2000-01-1633, 2000.

5. Falcone, P., F. Borrelli, J. Asgari, H.E. Tseng, and D. Hrovat, "Predictive Active Steering Control for Autonomous Vehicle Systems". Control Systems Technology, IEEE Transactions on, 2007. **15**(3): p. 566-580.

6. Falcone, P., H. Eric Tseng, F. Borrelli, J. Asgari, and D. Hrovat, "MPC-based yaw and lateral stabilisation via active front steering and braking". Vehicle System Dynamics: International Journal of Vehicle Mechanics and Mobility, 2008. **46**(1 sup.1): p. 611 - 628.

7. Falcone, P., M. Tufo, F. Borrelli, J. Asgari, and H.E. Tseng. "A linear time varying model predictive control approach to the integrated vehicle dynamics control problem in autonomous systems". 2008. Piscataway, NJ, USA: 2980-5, IEEE.

8. Hac, A. and M. Bodie, "Improvements in Vehicle Handling Through Integrated Control of Chassis Systems". Int. J. of Vehicle Autonomous Systems, 2002. **1**(1): p. 83-110.

9. Esmailzadeh, E., A. Goodarzi, and G.R. Vossoughi, "Directional stability and control of four-wheel independent drive electric vehicles". Proc Instn Mech Engrs Part K: J Multi-body Dynamics, 2002. **216**(4): p. 303-313.

10. Goodarzi, A. and E. Esmailzadeh, "Design of a VDC System for All-Wheel Independent Drive Vehicles". IEEE/ASME Transactions on Mechatronics, 2007. **12**(6): p. 632-639.

11. Karogal, I. and B. Ayalew, "Independent Torque Distribution Strategies for Vehicle Stability Control". SAE paper number 2009-01-0456, 2009.

12. Osborn, R.P. and T. Shim, "Independent Control of All-Wheel-Drive Torque Distribution". SAE paper number 2004-01-2052, 2004.

13. Piyabongkarn, D., J.Y. Lew, R. Rajamani, J.A. Grogg, and Q. Yuan, "On the Use of Torque-Biasing Systems for Electronic Stability Control: Limitations and Possibilities". IEEE Transaction on Control Systems Technology, 2007. **15**(3): p. 581-589.

14. Gradu, M., "Torque Bias Coupling for AWD Applications". SAE Paper No. 2003-01-0676, 2003.

15. Mohan, S.K. and A. Sharma, "Torque Vectoring Axle and Four Wheel Steering: A simulation Study of Two Yaw Moment Generation Mechanisms", in SAE World Congress, SAE Paper Number 2006-01-0819. 2006: Detroit, MI.

16. Kim, J., "Effect of vehicle model on the estimation of lateral vehicle dynamics". International Journal of Automotive Technology. **11**(No. 3): p. 331-337.

17. Kim, J. and H. Kim, "Electric Vehicle Yaw Rate Control using Independent In-Wheel Motor". IEEE, 2007: p. 705-710.

18. Ray, L.R., "Nonlinear state and tire force estimation for advanced vehicle control". Control Systems Technology, IEEE Transactions on, 1995. **3**(1): p. 117-124.

19. Ray, L.R., "Nonlinear Tire Force Estimation and Road Friction Identification: Simulation and Experiments". Automatica, 1997. **33**(10): p. 1819-1833.

20. Hongyan, G., C. Hong, and S. Tonghao. "Tire-road forces estimation based on sliding mode observer". in International Conference on.Mechatronics and Automation, 2009:p. 4577-4582.

21. Limroth, J., "Real-time Vehicle Parameter Estimation and Adaptive Stability Control", Ph.D Dissertation in Automotive Engineering. 2009, Clemson University: Clemson, SC.

22. Wanki, C., Y. Jangyeol, Y. Seongjin, K. Bongyeong, and Y. Kyongsu, "Estimation of Tire Forces for Application to Vehicle Stability Control". IEEE Transactions on Vehicular Technology, **59**(2): p. 638-649.

23. Fukada, Y., "Slip-Angle Estimation for Vehicle Stability Control". Vehicle System Dynamics: International Journal of Vehicle Mechanics and Mobility, 1999. **32**(4): p. 375 - 388.

24. Kim, J., "Identification of lateral tyre force dynamics using an extended Kalman filter from experimental road test data". Control Engineering Practice, 2009. **17**(3): p. 357-367.

25. Genta, G., Motor Vehicle Dynamics: Modeling and Simulation. Series on Advances in Mathematics for Applied Sciences. Vol. 43. 1997, Singapore: World Scientific

26. Gillespie, T., Fundamentals of Vehicle Dynamics. 1992: SAE,Warrendale, PA.

27. Milliken, W.M.a.D., Race Car Vehicle Dynamics. 1995, SAE, Warrendale, PA

28. Wong, J.Y., Theory of Ground Vehicles. 1993, New York, NY: John Wiley & Sons.

29. National Highway Traffic Safety Administration (NHTSA), D., "Federal Motor Vehicle Safety Standards; Electronic Stability Control Systems; Controls and Displays; 49 CFR Parts 571 and 585". 2007.

30. Pacejka, H.B., Tyre and Vehicle Dynamics. 2002, Oxford: Butterworth-Heinemann.